

ANALYSIS OF PAN-STARRS PHOTOMETRIC AND ASTROMETRIC DATA FOR DATA ASSOCIATION AND PHYSICAL CONSISTENCY ASSESSMENT

Tom Kececy⁽¹⁾, Moriba Jah⁽²⁾, Paul Sydney⁽³⁾, Paul Kerwin⁽⁴⁾

⁽¹⁾ *The Boeing Company, 5555 Tech Center Drive, Ste. 400, Colorado Springs, CO 80919, USA, Email: Thomas.M.Kececy@boeing.com*

⁽²⁾ *Air Force Research Laboratory (RV), 3550 Aberdeen Ave., SE, Kirtland AFB, NM 87117, USA*

⁽³⁾ *Pacific Defense Solutions (PDS), 1300 N. Holocono St., #116, Kihei, HI 96753, USA, Email: Paul.Sydney@pacificds.com*

⁽⁴⁾ *Air Force Research Laboratory (RD), 535 Lipoa Pkwy., Ste. 200, Kihei, HI 96753, USA*

ABSTRACT

Pan-STARRS data collected on several periods in 2010 are analyzed. The Constrained Admissible Region Multiple Hypothesis Filter process is applied to the optical angle (astrometric) data in an attempt to associate tracklets to unique objects. All tracklets have corresponding magnitude data associated with them. The magnitudes corresponding to the associated data are analyzed for consistency between the tracklets to gain some insight into the magnitude characteristics. The eventual goal is to fuse astrometric and photometric data in a way that enables a more comprehensive characterization of an object, including orbit, attitude, shape, and material composition. The results show some consistency between associated tracklets, but not in all cases.

1 INTRODUCTION AND BACKGROUND

The Panoramic Survey Telescope and Rapid Response System (Pan-STARRS) is a telescope designed and built by the University of Hawaii Institute for Astronomy for an astronomical mission. The prototype telescope system (PS1) is located at the 3000 meter summit of Haleakala on the island of Maui, in Hawaii. Although the system was designed for astronomical purposes, with a sidereal tracking mode, it can be used for observing Earth-orbiting satellites by turning the tracking mode off, staring at a fixed azimuth and elevation. This effectively optimizes the observations for satellites in geostationary orbit (GEO), but tracks for near GEO objects may also be obtained. PS1 photometric and astrometric data have been collected and processed in a preliminary fashion, but have not yet been thoroughly analyzed to determine which tracks might be associated to each other, and hence, associated with a specific debris object. This underscores one of the greatest challenges for the management of the potentially large quantities of observed space debris tracks: the association of collected and uncorrelated data to be used for characterizing unknown and

unresolved space objects. The most efficient and timely approach would utilize both the photometric and astrometric information available for the tracks to perform the association and derive physical attributes.

The purpose of the work presented in this paper is to take the first step in demonstrating the presumed physical relationship between photometric variations in the observed PS1 data and variations in albedo-area-to-mass ratio ($C_r A/m$) estimates derived from the astrometric data. This is due to the shape and attitude variations that are observed in the photometric time histories also being related to the albedo-area-to-mass ratio variations derived from the astrometric data, the result of solar radiation pressure effects. The Constrained Admissible Region Multiple Hypothesis Filter (CAR-MHF) is used to initialize and associate the astrometric tracks collected by PS1. The orbit and albedo-area-to-mass ratio values are estimated, and the resulting orbital elements are plotted to view the distribution of the observed debris orbits and albedo-area-to-mass ratio attributes. The photometric brightness statistics for all associated tracks on a given object are then tabulated. The brightness average and associated variations are subsequently compared to the average and variations of the albedo-area-to-mass ratios estimated for the same object.

The ultimate goal is to derive models of the physical relationships between the two measurement types with the intent of eventually combining them in a process that would derive estimates of physically interdependent attributes. This should yield, not only better and more consistent object attributes, but also more accurate predictions and uncertainties needed for follow-up observations and characterization.

2 PAN-STARRS DATA

The Pan-STARRS 1 (PS1) telescope, in operation since 2009 atop Haleakala on the Island of Maui, has provided 23rd visual magnitude (M_v) or better sensitivity and sub arc-second metric accuracy when

tracking in stare mode (i.e. frozen orientation with respect to an Earth-Fixed frame) or sidereal track mode (i.e. following the stars). The PS1 system is a wide-field-of-view (WFOV) sensor designed for the detection of near-Earth objects (NEO) which could pose a threat to our planet; it was funded and developed collaboratively by the University of Hawaii Institute for Astronomy and the Air Force Research Laboratory (AFRL). As a consequence, AFRL was given observing time on the system to demonstrate the utility of the system achievable for tracking dim, Earth-orbiting objects such as debris.

The approximate visual magnitude limit at GEO of most ground-based surveillance systems is 17 Mv. Given that a system such as PS1 can detect objects much dimmer, it is reasonable to assume that there will be objects detected by PS1 which have never been “seen” before. Therefore, one critical goal is to determine a Concept of Operations (CONOPS) that accommodates the expected density of objects that will be detected, primarily in the GEO regime. The WFOV of around 4 degrees, combined with sub-arc second astrometric tracking accuracy, provides a valuable resource for development and demonstration of techniques to help improve our ability to monitor the deep-space objects near GEO.

The challenge is to adopt a survey and tracking scheme that does the best job of identifying and discriminating dim objects of interest buried within the data that are collected (both astrometry and photometry) for all of the detected objects in a given set of frames. Traditionally data on detected objects must be properly associated with those objects a priori in order to perform an initial orbit determination (IOD) and follow-up tracking in order to successfully characterize them.

The PS1 telescope was used to collect and process images in 2010, 2011 and 2012 in an effort to find near GEO debris objects, and to demonstrate the “utility” of using a wide-field-of-view telescope to acquire and track deep-space objects. The data analyzed for the work presented here was collected in May 7-8, 2010, and September of 2010. Data “tracklets” spanning several minutes and having data separated by a minute or two were collected while in stare mode. The distribution of average absolute magnitudes for the data tracklets collected over May 7-8 is shown in Figure 1, while the variation in magnitudes for the tracklets is provided in Figure 2. The magnitude distribution shows the expected bi-modal signature with peaks in the low (bright) and high (dim) regimes. The variations within the tracklets are typically 0.5 or less, though there are some variations that go as high as 2.

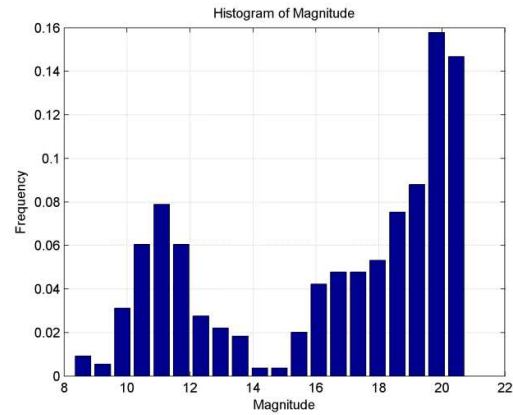


Figure 1. Distribution of absolute magnitudes for all objects observed over May 7-8, 2010.

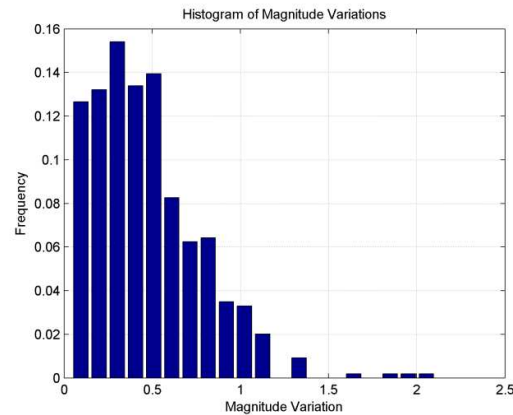


Figure 2. Distribution of absolute magnitude variations for all objects observed over May 7-8, 2010.

3 DATA ANALYSIS SUMMARY

The analysis conducted, and presented here, began by applying CAR-MHF to the PS1 data over selected periods of May 7-8, and September 2-27 of 2010. The sparseness of associated tracks was evident in most all of the results, but there were cases of successful association of tracklets. In the case of the May data, 3 data criteria were used for assessment: (1) tracklets having visual magnitudes in the range 8-14 (“low mag”), (2) tracklets having visual magnitudes in the range of 14-19 (“mid mag”), and (3) objects having high visual magnitudes (“hi mag”). The higher the visual magnitude, the dimmer the apparent object is. An object for which there were sufficient data associations and subsequent orbit estimates was selected from each of these categories for the consistency analysis. In addition, a HAMR object was also analyzed. The CAR-MHF processing results are presented in the following section, and magnitude consistency analysis in the section following that one.

4 CAR-MHF PROCESSING

The CAR-MHF processing flow is illustrated in Figure 3. The CAR process [1,2] initiates a set of filters when no existing estimates are available to process (i.e. when the available data are not associated to previously known objects, also called Un-Correlated Tracks [UCTs]). Existing estimates may be available from previous CAR generations. The CAR initiates a set of hypotheses based on UCT data alone (i.e. absent *a priori* state vector information) and user supplied hypothesis constraints. Each hypothesis is propagated to the next measurement time, at which point a probabilistic data association process is applied to one or more data pairs that might occur at a single time. If any measurements are associated to any hypotheses (based upon a Mahalanobis Distance criterion), all hypotheses for that object are updated with the associated measurement, and those updated are weighted based on their statistical likelihood as presented in [3,4]. In the case of an update, the hypothesis weights are adjusted accordingly and pruned based on user-selected criteria. If no update occurs, the hypotheses weights remain unchanged.

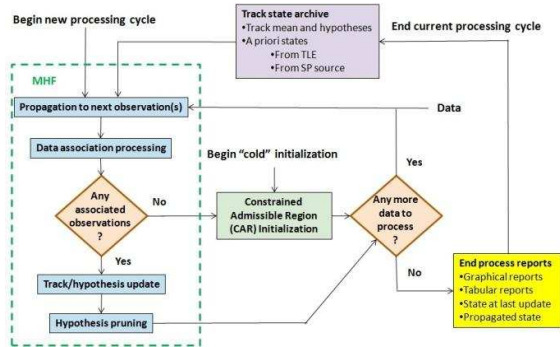


Figure 3. Depiction of the CAR-MHF process flow.

Conceptually, the data and hypothesis update approach enables multiple data to inform the filter which hypotheses are the most likely states. Each filter update further refines the hypotheses, rejecting the least likely, so ultimately the surviving hypothesis (or couple of hypotheses) yields the converged state estimate. The method can be thought of as an inductive process where states are hypothesized and the data are exploited for their ability to identify those hypothesized states that are statistically unlikely. It allows the user to only infer trajectories that are able to predict future observations. This process is depicted in Figure 4, where it should be noted that the Mahalanobis distance metric is the basis for the data association. Each hypothesis state and covariance at the measurement time is mapped to measurement space (“C” and “P” in Figure 4) and compared to the actual measurement at that time (“O” in Figure 4). The k^2 parameter is a chi-squared statistic

that is compared against a user-specified probability limit (and is only statistically valid for distributions that are sufficiently Gaussian).

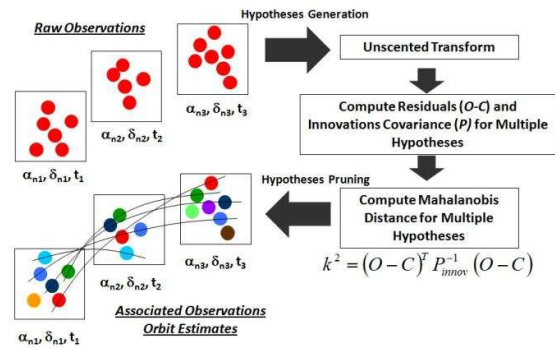


Figure 4. Conceptual depiction for multiple hypothesis and multiple data association processing.

An example of the CAR generated for the low magnitude object for the May 7-8 data is shown in Figure 5 where the left-hand plot shows the CAR range versus range-rate region derived from an initial tracklet and the near GEO constraints. The right-hand plots show the hypothesized orbital elements for eccentricity versus semi-major axis (top), inclination versus semi-major axis (middle), and right ascension of ascending node versus semi-major axis (bottom). The plots for the mid, high, and HAMR objects are similar. Only the HAMR object had an additional SRP hypothesis as the May 7-8 do not span sufficient amount of time to have a chance of adequately estimating the SRP.

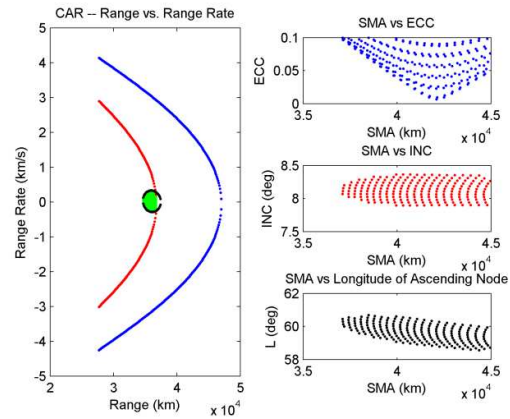


Figure 5. CAR generation for example object in low magnitude category (May 7-8, 2010 processing).

The hypotheses represented in Figure 5 are processed by the MHF and, where detected, associated data/tracklets are used to update the states and subsequently “weak” hypotheses are pruned. The estimation updates over the 2-day span are shown in Figures 6-9 for the low, mid, high, and HAMR objects, respectively

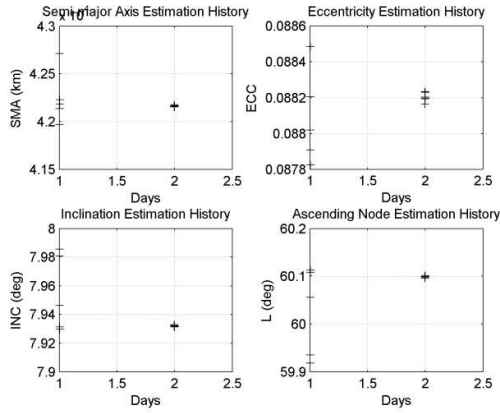


Figure 6 Orbital element estimates for example object in low magnitude category (May 7-8, 2010 processing).

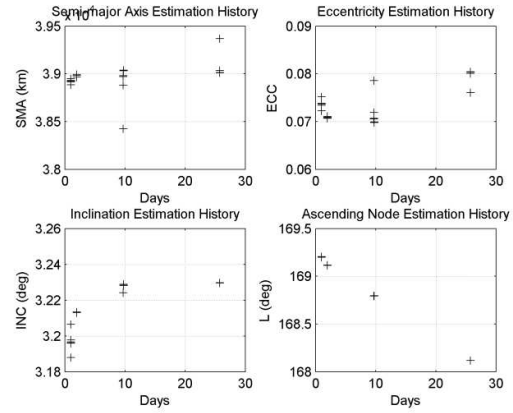


Figure 9 Orbital element estimates for example HAMR object (September 2-27, 2010 processing).

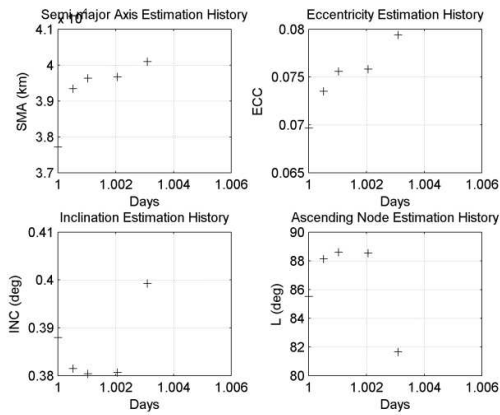


Figure 7 Orbital element estimates for example object in mid magnitude category (May 7-8, 2010 processing).

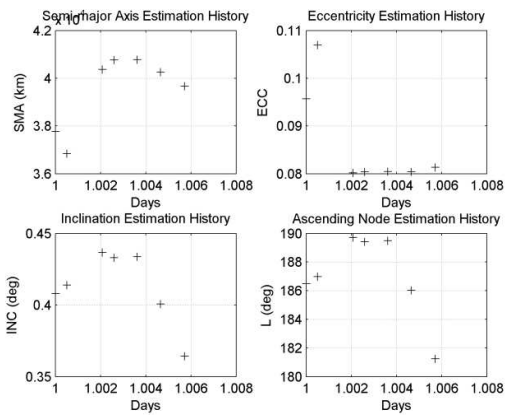


Figure 8 Orbital element estimates for example object in high magnitude category (May 7-8, 2010 processing).

As indicated in the plots, the data that were associated were sparse and so limited updates were performed. More details of the data association results, along with the magnitude consistency analysis for these four cases, is presented in the following section.

5 DATA ASSOCIATION AND CONSISTENCY ANALYSIS

To gain insight into the analysis that follows, the magnitudes for the three brightness categories are analyzed for the May 7-8 data. Figure 10 shows the magnitude distribution for the “low mag” tracklets which ranges from 8-14, and peaks around 11. The corresponding magnitude variations are provided in Figure 11 and are generally less than an order of magnitude.

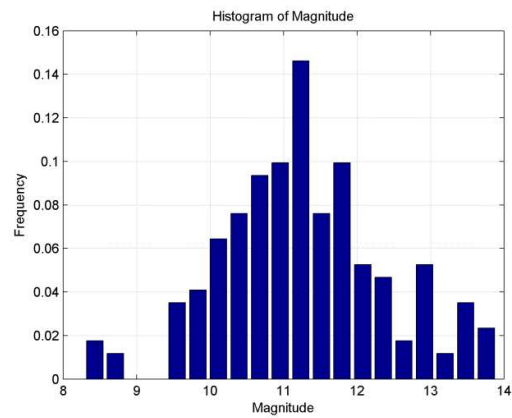


Figure 10 Distribution of absolute magnitudes for low magnitude category.

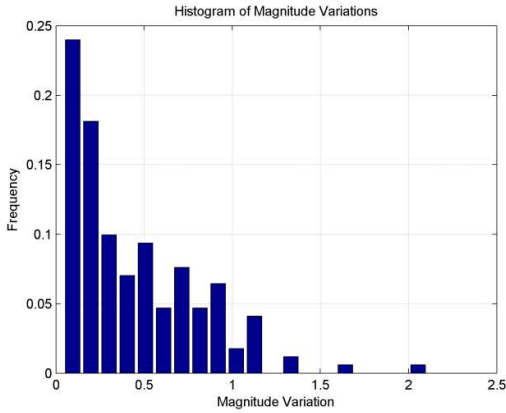


Figure 11 Distribution of absolute magnitude variations for low magnitude category.

Figure 12 shows the magnitude distribution for the “mid mag” tracklets which ranges from 14-19, with most of them falling in the range of 16-19. The corresponding magnitude variations are provided in Figure 11 and are also less than an order of magnitude, though there are a few variations near 2 orders of magnitude.

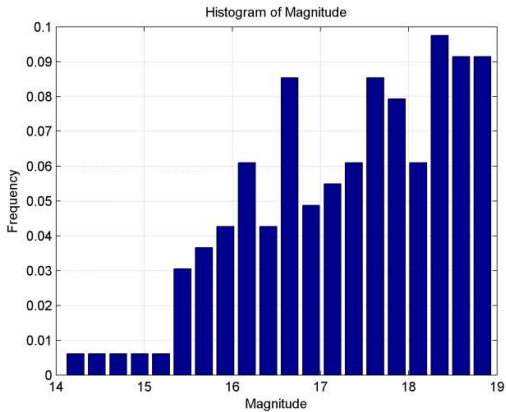


Figure 12 Distribution of absolute magnitudes for mid magnitude category.

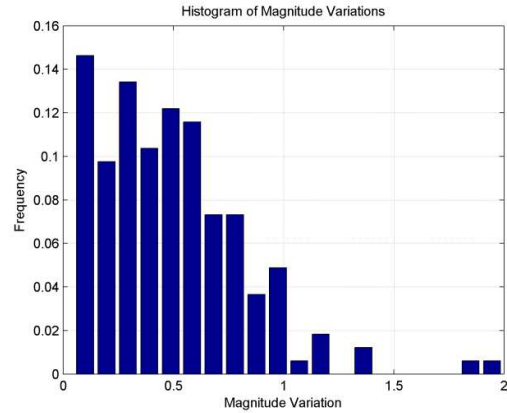


Figure 13 Distribution of absolute magnitude variations for mid magnitude category.

Finally, Figure 14 shows the magnitude distribution for the “hi mag” tracklets which ranges from 19-21, with a slight dip in the distribution around 19.5. The corresponding magnitude variations are provided in Figure 15 and are also less than an order of magnitude, though there are a few variations near 2 orders of magnitude. Note also the intriguing peak in the distribution around magnitude variation 0.4.

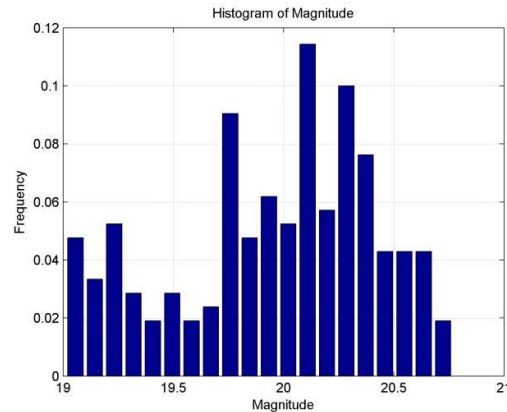


Figure 14 Distribution of absolute magnitudes for high magnitude category.

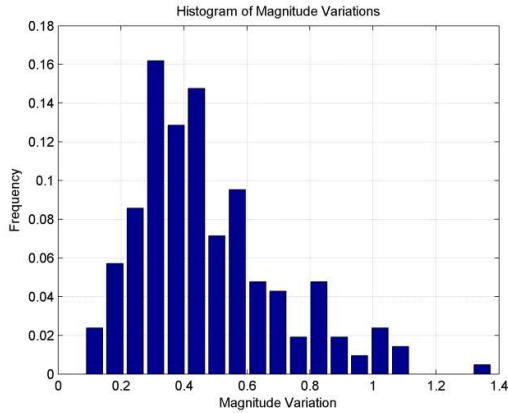


Figure 15 Distribution of absolute magnitude variations for high magnitude category.

A summary of the associated data and tracks resulting from the CAR-MHF processing of the astrometric data is provided in Table 1 for the low, mid and high magnitude object categories. The total number of observations ranges from 150 to 157, and the number of these observations that are actually associated is 35 to 74. The total number of tracks that were initialized by CAR ranges from 23 to 26, and of these, only 4 to 7 successful associations. This relatively low success rate is attributed to the observing strategy which was not necessarily focused on capturing follow-up measurements on objects.

Table 1. The resulting associated data and tracks are provided for the low, mid and high magnitude observation categories.

Magnitude Category	Total # Obs	Total Obs Associated	Total # Tracks	# Tracks Associated
Low	157	67	24	6
Mid	153	35	26	4
High	150	74	23	7

Table 2 below summarizes the consistency results. The categories provide a summary for each of the four objects that were analyzed. The number of starting hypotheses ranged from 151 for the HAMR object to 262 for the high magnitude object. Only the HAMR object had sufficient data to converge to a single hypothesis, while the mid magnitude object only had sufficient data to converge to 68 hypotheses (i.e. one would not consider this a stable orbit solution and the number of surviving hypotheses indicates this ambiguity). The semi-major axis for the mid magnitude, high magnitude, and HAMR objects are all sub-synchronous orbits, while the low magnitude (bright) object is obviously very close to GEO. The eccentricities range from 0.0167 to 0.0804, and

inclinations from 0.203 degrees to 7.957 degrees.

Each of the four objects has a set of “tracks” that were associated with it (i.d. in the far left column). The number of astrometric observations associated for each of the objects was 15-16 for the objects reduced from the May 7-8 data, and 33 for the HAMR object. The last two columns show the mean and variation of the magnitudes for each of the tracklets. It can be seen that the low, high, and HAMR objects show fairly good magnitude consistency between each of the corresponding tracklets in each of those categories. However, the mid magnitude object resulted in a fairly high variation between the two means. This could be a result of variations in the ranges (magnitudes are un-normalized), attitude variations, or there is also the possibility that the tracklets were in fact not truly originated from a unique object. Subsequent data would be needed to resolve this potential inconsistency.

Table 2. Below is a summary of the 4 near GEO objects for which data association and magnitude consistency were performed. The objects are categorized as “low magnitude,” “mid magnitude,” “high magnitude,” and “HAMR.”

Track Assoc	Category	Start Hyp.	End Hyp.	#Obs Assoc.	Sma (km)	Ecc.	Inc. (deg)	CrA/m (m ² /kg)	Mean Mag	Var. Mag
90202	Low mag	219	3	15	42156.865	0.0785	7.957	0.049	8.479	0.765
90151									8.771	0.839
90425									8.293	0.185
90009	Mid mag	258	68	15	40351.932	0.0339	0.277	0.049	18.114	0.392
90357									16.292	0.575
90028	High mag	262	24	16	39715.709	0.0167	0.203	0.049	19.077	0.301
90360									19.198	0.849
90316									20.247	0.437
90579									20.084	0.218
90591	HAMR	151	1	33	39011.179	0.0804	3.230	10.219	19.877	0.244
20002									20.799	0.493
90683									20.418	0.412
90689									20.299	0.318
90574									20.523	0.191

More insight is provided into the magnitude histories for the cases summarized in Table 2. The magnitudes as a function of observation number are given in Figures 16-19 for the low, mid, high, and HAMR cases, where each tracklet for each of the objects has been assigned a unique color to distinguish them. The low magnitude object history (Figure 16) looks fairly consistent between each of the 3 tracklets with an average magnitude of 8.514 and standard deviation of 0.66. The mid-magnitude object history (Figure 17) is less consistent between each of the 2 tracklets with an average magnitude of 17.51 and standard deviation of 1.1. The high magnitude object history (Figure 18) has some structure, though the values are again fairly less consistent with an average magnitude of 19.45 and standard deviation of 0.72. Finally, the HAMR object magnitude history (Figure 19) seems the most consistent with an average of 20.31 and standard deviation of 0.42. In all cases there are occasional “outliers,” which are likely artefacts of either the image processing that was applied, or possibly glints.

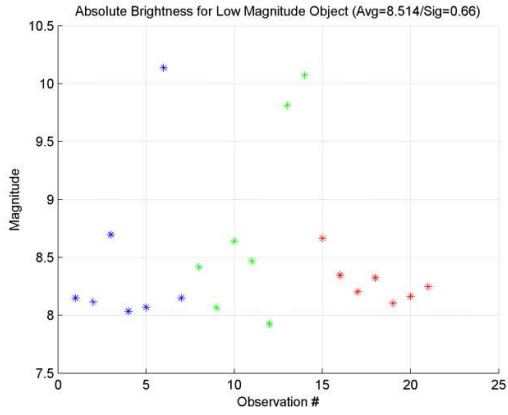


Figure 16 Absolute magnitude vs. observation number for low magnitude object (3 tracks uniquely colored).

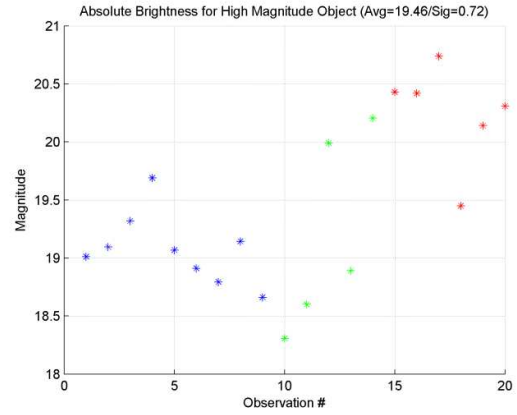


Figure 18 Absolute magnitude vs. observation number for high magnitude object (3 tracks uniquely colored).

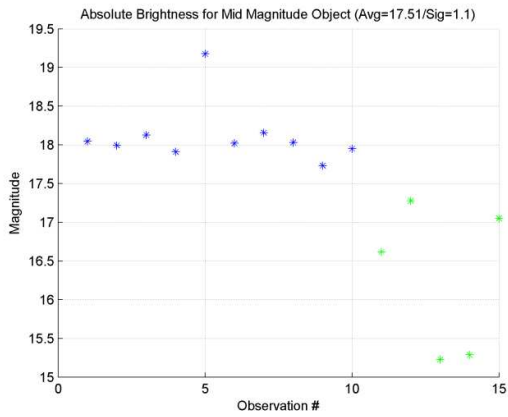


Figure 17. Absolute magnitude vs. observation number for mid magnitude object (2 tracks uniquely colored).

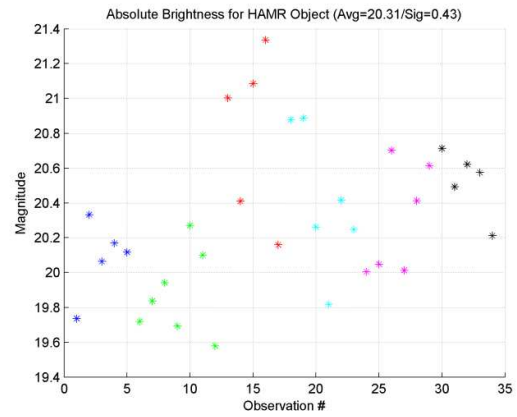


Figure 19 Absolute magnitude vs. observation number for HAMR object (6 tracks uniquely colored).

6 SUMMARY AND CONCLUSIONS

Data collected by PS1 at various times in 2010 were analyzed over specific periods (May 7-8 and September 2-27). The CAR-MHF process was run in an attempt to autonomously assess if any of the tracklets were associated to unique objects. The absolute magnitudes for those tracklets that appeared to be associated with a given object were then analyzed for consistency. Though it is acknowledged that magnitude can vary by several orders of magnitude, the magnitude variations for each set of associated observations appeared to be relatively limited and showed consistency amongst the associated tracklets. More data should be collected in a fashion which insures repeat visits to objects. The results indicate fusion of astrometric and photometric data might be beneficial to characterization of unknown space debris objects.

7 ACKNOWLEDGEMENTS

This work was funded by the Air Force Research Laboratory. We would like to acknowledge the support of those who collected the PS1 data. A huge thank you also goes to those who worked in a timely fashion to get this paper through the public release process in time to be presented at the conference.

8 REFERENCES

1. Milani, A., G. Gronchi, M.D.M. Vitturi and Z. Knezevic (2004). Orbit Determination with Very Short Arcs. I Admissible Regions. *Celestial Mechanics and Dynamical Astronomy*, Vol. 90, July 2004, pp59-87.
2. Kelecy, T., M. Jah and K. DeMars (2012). Application of a Multiple Hypothesis Filter to near GEO high area-to-mass ratio space objects state estimation. *Acta Astronautica*, 81, pp 435-444.
3. DeMars, K., M. Jah and P. Schumacher (2012). Initial Orbit Determination using Short-Arc and Angle Rate Data. *IEEE Journal of Transactions on Aerospace and Electronic Systems*, Volume 48, Number 3, July 2012.
4. Julier, S. and J. K. Uhlmann (1997). A New Extension of the Kalman Filter to Nonlinear Systems. *Proceedings of the SPIE – The International Society for Optical Engineering*, Vol 3068, April 1997, pp 182-193.